Applied Surface Science 389 (2016) 1126–1136

Contents lists available at ScienceDirect

Applied Surface Science

journal homepage: www.elsevier.com/locate/apsusc

Passive behaviour of alloy corrosion-resistant steel Cr10Mo1 in simulating concrete pore solutions with different pH

Zhiyong Ai[a,b], Jinyang Jiang[a,b], Wei Sun[a,b,*], Dan Song[a,b,c], Han Ma[d], Jianchun Zhang[d], Danqian Wang[a,b]

[a] School of Materials Science and Engineering, Southeast University, Nanjing 211189, Jiangsu, China
[b] Jiangsu Key Laboratory of Construction Materials, Nanjing 211189, Jiangsu, China
[c] College of Mechanics and Materials, Hohai University, Nanjing 210098, Jiangsu, China
[d] Research Institute of Jiangsu Shasteel Iron and Steel, Zhangjiagang 215625, Jiangsu, China

ARTICLE INFO

Article history:
Received 5 May 2016
Received in revised form 19 July 2016
Accepted 22 July 2016
Available online 1 August 2016

Keywords:
Corrosion-resistant steel
Passive behaviour
Film composition
pH

ABSTRACT

The passive behaviour of new alloy corrosion-resistant steel Cr10Mo1 and plain carbon steel (as a comparison) in simulating concrete pore solutions of different pH (ranging from 13.5 to 9.0) under open circuit potential conditions, was evaluated by various electrochemical techniques: potentiodynamic polarization, capacitance measurements and electrochemical impedance spectroscopy. The chemical composition and structure of passive films were investigated by X-ray photoelectron spectroscopy (XPS) and secondary ion mass spectroscopy (SIMS). The electrochemical responses of passive films show that Cr10Mo1 steel has an increasing passivity with pH decreasing while carbon steel dose conversely, revealing carbonation does no negative effect on passivation of the corrosion-resistant steel. SIMS reveals that the passive film on the corrosion-resistant steel presents a bilayer structure: an outer layer mainly consisting of Fe oxides and hydroxides, and an inner layer enriched in Cr species, while only a Fe-concentrated layer for carbon steel. According to the XPS analysis results, as the pH decreases, more stable and protective Cr oxides are enriched in the film on Cr10Mo1 steel while Fe oxides gradually decompose. Higher content of Cr oxides in the film layer provides Cr10Mo1 corrosion-resistant steel more excellent passivity at lower pH.

1. Introduction

As is well known, reinforced concrete is a versatile and economical construction material, which is widely-used in civil infrastructures. However, steel corrosion in concrete caused by aggressive species such as chlorides and carbon dioxide, occasions cracking of the concrete cover and concomitant deterioration in the mechanical performances, leading to premature failure of concrete structures [1]. By far, for reinforcing steel corrosion problems, a wide variety of protection and repair methods have been applied, such as increasing concrete cover quality and thickness, using special steel rebar (stainless steel, galvanizing rebar, epoxy coated steel reinforcement, etc), incorporation of inhibitors during concrete mixing, electrochemical protection (including cathodic protection, electrochemical realkalization and electrochemical chloride extraction) [2,3], using fiber reinforced plastic in substitution for steel [4], migrating corrosion inhibitors to reinforcing steel through concrete cover [5]. However, these techniques all have their own disadvantages and are subject to some limitations, and more efficient solutions for steel corrosion are required.

Prompted by massive and rapidly rising construction and maintenance costs, civil engineering designers have proposed a design service life goal of 75–100 years [6] for concrete structures under severe conditions without major repairs. Nowadays, cathodic protection and using stainless steel as rebar seem to be the most reliable measures to prevent steel corrosion persistently and guarantee the durability of concrete structures in highly aggressive environments. Some researchers [7] have shown, using stainless steel reinforcements with surpassing corrosion resistance can be, in the long term, a more economically profitable alternative than cathodic protection which requires continuous maintenance. However, stainless steels have quite high level of alloying elements

* Corresponding author at: School of Materials Science and Engineering, Southeast University, Nanjing 211189, Jiangsu, China.
E-mail addresses: 230139452@seu.edu.cn (Z. Ai), jiangjinyang16@163.com (J. Jiang), sunwei@seu.edu.cn (W. Sun), songdancharls@hhu.edu.cn (D. Song), mahan-iris@shasteel.cn (H. Ma), Zhangjc-iris@shasteel.cn (J. Zhang), wonderbaba@126.com (D. Wang).

http://dx.doi.org/10.1016/j.apsusc.2016.07.142
0169-4332/

(≥12% Cr and ≥8% Ni, or ≥20% (Cr + Ni)), resulting in high initial cost, which limits their wide use [8,9].

Over the past dozen years, low-alloy corrosion-resistant steels have been developed, which as promising reinforcements have considerably high corrosion resistance but more attractive economy than stainless steels, such as fine-grained Cu-P and Cu-Cr-Ni alloy steel [10,11], MMFX steel [12], etc. Among of them, MMFX is the most significant one. The so called "MMFX" steel is Microcomposite Multi-structural Formable Steel developed by MMFX Steel Corporation, USA, in 1998, and is claimed by its innovators to have a significantly high corrosion resistance but moderate added cost and superior mechanical properties, compared to conventional carbon steel. This alloy has about 9.0 wt.% Cr with small amounts of Mo and Ni, and is almost carbon free (carbon content is limited to 0.15 wt.% maximum in the ASTM C1035A/1035M-04 specification), consisting of dislocated martensite laths with untransformed austenite between the laths, with no carbides almost which are cathodic to the matrix [13]. It is reported that MMFX steel has a corrosion resistance 5–6 times better than that of conventional carbon steel (ASTM A615) as measured by the critical chloride threshold level [14,15], and can extend the service life of concrete structures for several decades [16,17]. However, generally, it seems that it is difficult to achieve the service life goal of 75–100 years for concrete structures using MMFX steel as reinforcements, and new tailored low-alloy steels with higher corrosion resistance need to be developed. Since 2008, Research Institute of Jiangsu Shasteel Iron and Steel has been committed to develop and research new alloy steels with high corrosion resistance and strength. Of them, one named "Cr10Mo1", with Cr about 10 wt.% and Mo about 1 wt.%, and yield strength above 400 MPa, which has similar chemical composition but very different metallurgical microstructure compared to MMFX steel, was prepared out and has been successfully declared for Chinese invention patents [18]. Preliminary corrosion accelerated tests in laboratory showed that Cr10Mo1 steel has a critical chloride threshold level more than 10 times that of plain carbon steel, showing more anticorrosive than most of common alloy corrosion-resistant steels in the past. Cr10Mo1 steel may bring about potential longer service life of concrete structures but without significant increasing costs compare to MMFX steel, owing to its higher corrosion resistance. For the steel to be acceptable to the concrete community, a number of detailing characteristics about the corrosion behavior of such steel must be determined.

Similar to MMFX steel, Cr10Mo1 steel having excellent corrosion resistance may be attributed to the presence of a strongly protective film formed essentially by iron and chromium oxides on the metal in alkaline media. However, systematic studies focused on the passive behaviour of alloy corrosion-resistant steels in different pH conditions are scarce. The present work aims at studying the passivation of alloy corrosion-resistant steel Cr10Mo1 in conditions simulating the fresh and carbonated concrete pore solutions chemistry, to ascertain the effects of pH on the composition and characteristics of surface film formed on the steel.

2. Experimental procedures

2.1. Materials

2.1.1. Test solutions

Based on the reports [19,20], an aqueous calcium-sodium-potassium hydroxide solution with 0.3 M $Ca(OH)_2$ (saturated) + 0.5 M KOH + 0.2 M NaOH (pH 13.5), prepared with analytical grade chemicals and Millipore water (18.2 MΩ cm), was used to simulate the interstitial electrolyte of concrete pores.

Solutions with lower pH (12.0, 10.5, 9.0) were prepared by addition of $NaHCO_3$ powder into the 0.03 M $Ca(OH)_2$ (saturated) solution (pH about 12.5) [21], to simulate the carbonation process which could decrease the pH of concrete pore solution down to values close to 9.0. The detailed procedure and quantities to prepare the solutions of all pH are listed in Table 1. The pH of the solutions was carefully checked and monitored throughout by a pH meter (Thermo Scientific Orion pH2100).

Table 1
Composition and pH of the simulated concrete pore solutions.

Solution	Composition (M)				pH
	$Ca(OH)_2$ (sat.)	KOH	NaOH	$NaHCO_3$	
1	0.03	0.5	0.2	–	13.5
2	0.03	–	–	0.038	12.0
3	0.03	–	–	0.054	10.5
4	0.03	–	–	0.149	9.0

Table 2
The chemical composition of CR and PC steel.

Type	Chemical composition (wt.%)								
	Fe	C	Si	Mn	P	S	V	Cr	Mo
CR	Bal.	0.01	0.49	1.49	0.01	0.01	0.06	10.36	1.16
PC	Bal.	0.22	0.53	1.44	0.02	0.02	0.04	–	–

2.1.2. Steel samples

Experimental materials were the newly designed alloy corrosion-resistant HRB400 steel Cr10Mo1 (CR), provided by Research Institute of Jiangsu Shasteel Iron and Steel, and plain carbon HRB400 steel (PC) (as a comparison). The chemical composition of CR and PC steel studied is given in Table 2.

Optical Microscopy (OM) images of the etched cross sections obtained for CR and PC steel are shown in Fig. 1. The microstructure of CR steel consists of granular bainite with ferrite between the grains. PC steel shows typical hypo-eutectoid microstructure, made up of ferrite and fine pearlite with carbides distributed within the matrix and at the boundaries.

Steel samples of 10 mm length were cut from ribbed rebars with a diameter of 25 mm. The cross-sections of steel samples were ground with grades 200, 600, 1000 and 2000 silicon carbide emery papers successively, and polished with alumina paste up to 2.5 μm grit to eliminate the heterogeneities of the steel surface. After polishing, the samples were degreased subsequently with alcohol, rinsed with distilled water and dried with a stream of air just before immersion, to ensure their same initial surface states. The samples were immersed in test solutions for up to 10 days to allow a mature/thick passive film to form during immersion [22].

2.2. Electrochemical measurements

The passivation progress with immersion time at different pH values was followed by electrochemical tests, performed at room temperature (25 °C) and under natural aeration in a classical electrochemical cell with a traditional three-electrode system. The steel sample as the working electrode was installed with an exposed working area of 1 cm^2, the reference electrode was a saturated calomel electrode (SCE, all electrode potentials reported in this study were referred to SCE), and platinum counter electrode was also used.

The potentiodynamic polarization tests were performed with ohmic potential drop compensation (taking account of the variation of test solutions resistance as pH changes) in the potential range from −0.2 V to +1.2 V vs. open circuit potentials (OCP) in the anodic direction at a scan rate of 0.5 mV/s after OCP stabilization. The electrochemical impedance spectroscopy measurements were carried out at in a frequency range from 10^4 Hz down to 10^{-2} Hz with an AC amplitude of 10 mV at OCP, and data integration was set

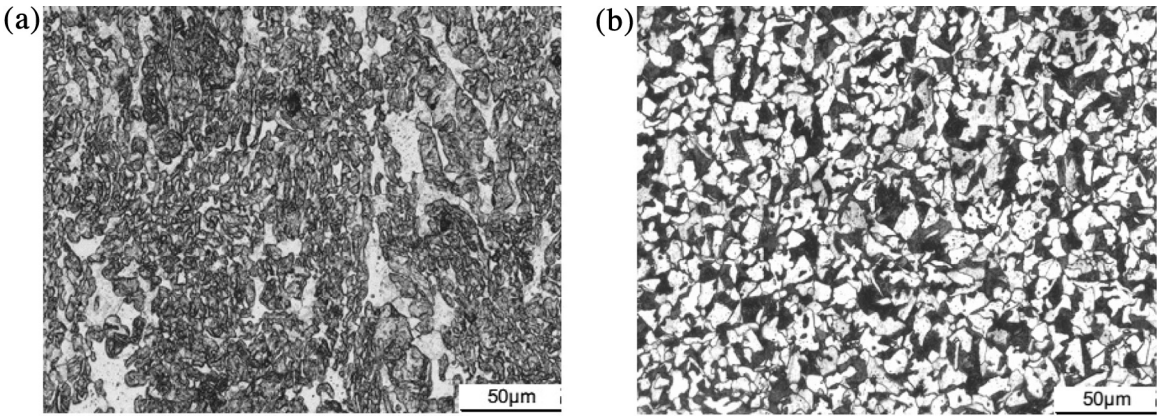

Fig. 1. Microstructure of the two steels obtained by OM: (a) CR and (b) PC.

at 5 steps per decade for the measurement. Mott-Shottky plot measurements were conducted at a fixed frequency of 1000 Hz and a sinusoidal signal of 10 mV was employed. The polarization was performed by successive steps of 50 mV in the cathodic direction in the potential range from +0.25 V to −1.5 V vs. SCE. There were 3 replicates for each specimen. The equipment used was a PARSTAT 4000 electrochemical system (Princeton Applied Research Inc., Oakridge, TN).

2.3. Surface analysis

2.3.1. XPS

The chemical composition of the films was determined by X-ray photoelectron spectroscopy (XPS). A PHI5000 Versa Probe spectrometer, equipped with a monochromatic Al Kα radiation source (1486.6 eV) and a hemispherical electron analyzer operating at a pass energy of 58.7 eV, was used. The XPS measurements were performed under pressures below 0.5×10^{-6} mbar, at successive steps of 0.125 eV. The curve fitting was performed by the commercial software XPSpeak version 4.1, which contained the Shirley background subtraction and Gaussian-Lorentzian tail function for better spectra fitting.

2.3.2. SIMS

The elemental distribution at discrete depths in the passive oxide layer on the steel substrate was investigated by secondary ion mass spectroscopy (SIMS) carried out with TOF. SIMS 5 (ION-TOF GmbH, Münster, Germany). Sputter ion beams of Cs^+ (1 keV impact energy, 10 nA beam current) was used (depending on the element to be analyzed) and rastered over a 200 μm × 200 μm square area to avoid crater edge effect. The measurements were carried out in ultra-high vacuum with a background pressure of $<5 \times 10^{-10}$ mba applied to prevent surface oxidation during the measurement.

3. Results and discussion

3.1. Surface analysis

3.1.1. XPS analysis

The chemical composition of the surface films formed on CR and PC steel at OCP in solutions of different pH (13.5–9.0) was examined by XPS. The results show that the mainly composition of passive film on CR steel is Fe, Cr and O (Fig. 2a), while mainly Fe and O for PC steel (Fig. 2b), indicating that in the alkaline solutions the primary constituents of the passive film are chromium oxides and iron oxides for CR steel while iron species for PC steel, respectively.

Deconvolutions of high resolution XPS spectra (Fe, Cr, O) were performed by a fit procedure described in previous papers [23,24], based on the corresponding binding energies reported in many literatures [23–25]. According to the binding energies, the Fe 2p ionisation is deconvoluted into three different contributions, which are assigned to Fe^{2+} in oxide (FeO, E_b = 709.5 eV) and Fe^{3+} in oxide (Fe_2O_3, E_b = 710.6 eV) and hydroxide form ($FeOOH/Fe(OH)_3$, E_b = 712.0 eV). The relative peak heights of Fe^{3+} in oxide separation in the Fe 2p spectra show that Fe_2O_3 is the primary Fe species in the passive film for CR and PC steel. There exist two constituent peaks in the Cr 2p signal, representing Cr^{3+} in oxide (Cr_2O_3, E_b = 576.3 eV) and hydroxide ($CrOOH/Cr(OH)_3$, E_b = 577.1 eV). The intensities of Cr^{3+} oxide state are apparently higher than that of Cr^{3+} hydroxide, indicating Cr_2O_3 is the dominant Cr species in the passive film for CR steel. Oxygen species play the role of connecting metal ions in passive film. The O 1 s spectrum shows the presence of two components: O^{2-} (E_b = 530.2 eV) and OH^- (E_b = 531.8 eV) states, corresponding to the formation of Fe/Cr oxides and hydroxides in the passive films.

The XPS measurements did not detect the presence of molybdenum in the passive film on CR steel, probably because separate molybdenum phase can not be formed in film for its too low content in steel substrate. Therefore, its effect will not be discussed in this paper. However, it is well known that Mo can ameliorate the defect structure of chromium species and therefore has an important effect on the electronic properties and corrosion resistance of the passive film as reported in previous studies [26].

Fig. 3 shows the cationic fractions in the passive films of the two steels as functions of the pH. The Fe^{2+}/Fe^{3+} ratio in passive film significantly decreases with pH for both CR and PC steel, suggesting that the passive films become depleted increasingly in magnetite (Fe_3O_4), which contributes substantially to Fe^{2+} species. This results are in agreement with previous works [21,27]. In fact, more alkaline media promote more Fe_3O_4 formation and maintain its stability [27]. When the surface film is exposed to lower pH, Fe_3O_4 decomposes gradually and transforms to porous $FeOOH/Fe(OH)_3$ with less protection [28], accompanied by a decrease of the Fe^{2+}/Fe^{3+} ratio. An important noteworthiness refers to the content evolution of Cr^{3+} in the film formed on CR steel. As the pH decreasing, there is a gradual enrichment in Cr species in the surface film. This fact may account for the higher stability of the Cr oxides insensitive to low pH values [24], in addition to the higher dissolution rate of Fe species at the film/solution interface when the pH drops according to the Pourbaix diagrams [28].

The increased content of Cr^{3+} combined with the decreasing Fe^{2+}/Fe^{3+} ratio in the surface film with pH dropping, evidences that the passive film on CR steel becomes richer in Cr species, meanwhile depleted gradually in Fe^{2+} oxide (This is also true for PC steel) when the pH drops.

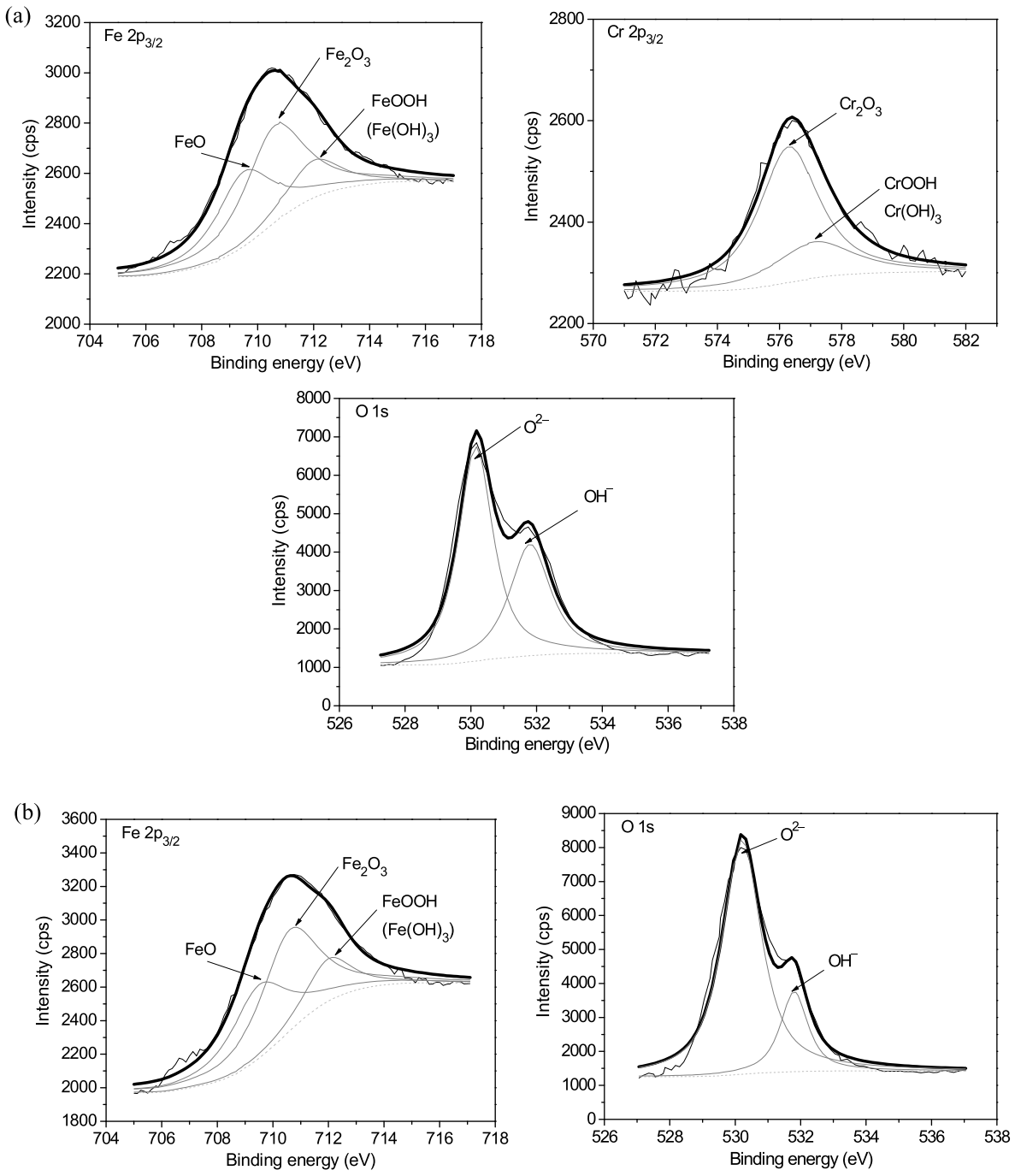

Fig. 2. XPS spectra for the surface films formed on the steels immersed in test solution of pH 13.5 for 3 d: (a) CR and (b) PC.

3.1.2. SIMS results

Compositional depth profiles through the matrix films on CR and PC steel were obtained using SIMS. Fig. 4, as an example, displays the relative concentration trends (log scale) of the ions such as $^{56}Fe^{16}O^-$, $^{12}C^-$, $^{52}Cr^{16}O^-$, $^{96}Mo^{16}O^-$ in the matrix oxides film. The usual horizontal scale of sputtering time has been converted to depth using the sputtering rate calculated for the matrix. According to Fig. 4, for CR steel, the FeO^-, CrO^- and MoO^- obey a certain layer stacking in the surface film. First, a high FeO^- intensity is detected in the uppermost layer. Thereafter, at about 3 nm around the middle of the oxide film, the CrO^- signal rises, and it is followed by the MoO^- signal (very weak). However, the CrO^- and MoO^- concentration decreases again closer to the substrate. It is assumed that a mixture of Fe–Cr spinel type oxides is formed on the alloy surface at the initial oxidation stage. When the oxidation proceeds, the Fe ions diffuse through the inner mixed spinel oxides and form the outer Fe-rich species because Fe ions are much more mobile than Cr and Mo ions [29]. Since the passive layer formation may deplete Cr and Mo at the metal/oxides interface [30], less free Cr and Mo remain available for incorporation into the network. For PC steel, only FeO^- signal is detected in the layer, indicating the passive film is a Fe-concentrated layer.

The depth profiles in Fig. 4 reveal that the distribution of Fe and Cr species within the surface film network covering the CR steel is similar to the oxides sequent stacking in the nm range in the passive films on Cr-series alloy steels reported in many studies [31,32]. Based on the interpretation of a layered stacking model, the passive film formed on Cr10Mo1 steel could also be described

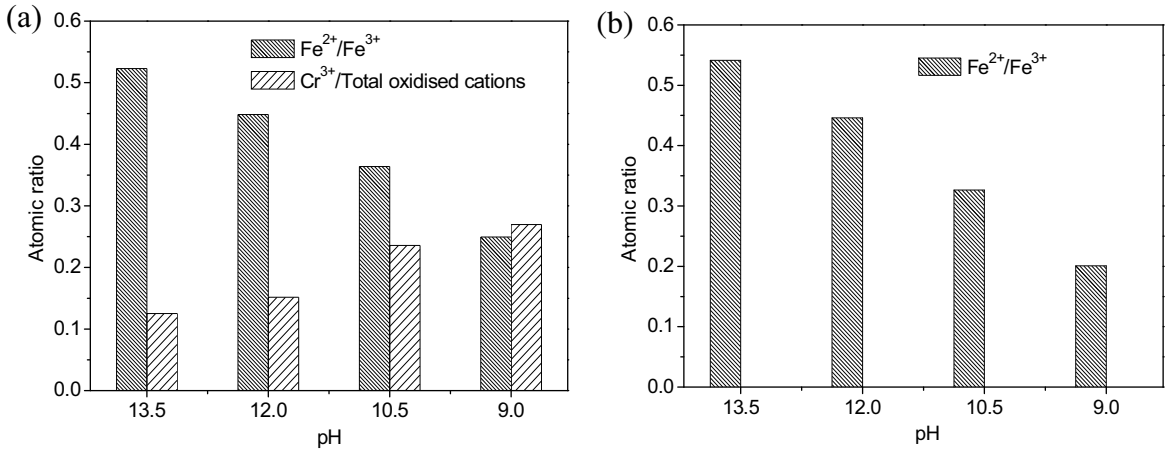

Fig. 3. The atomic ratios evolution of various cations presented in the passive films formed on the steels immersed in test solutions of different pH for 3 d obtained from quantitative XPS analysis: (a) CR and (b) PC.

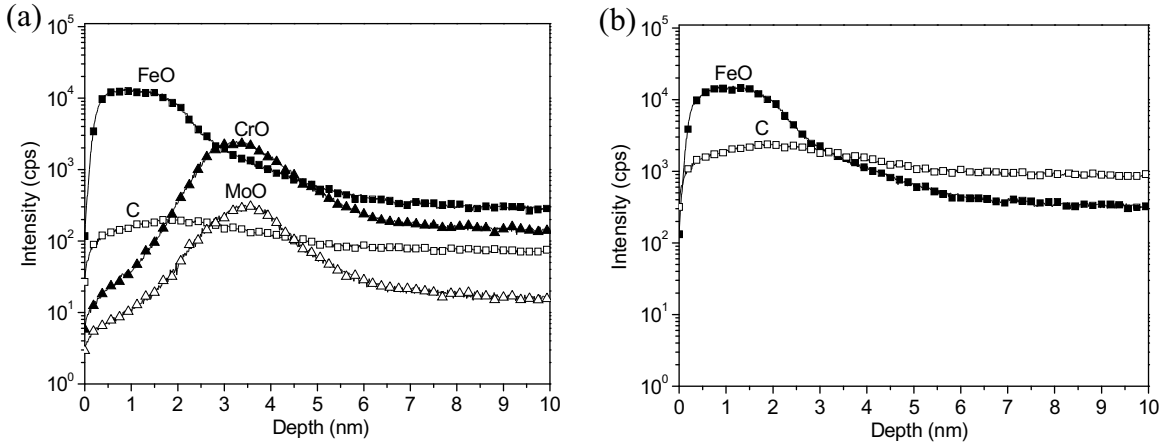

Fig. 4. Depth profiles addressing ions distribution in the passive films on the steels immersed in test solution of pH 13.5 for 3 d: (a) CR and (b) PC.

as a bilayer structure, composed of an outer layer, enriched in Fe species like Fe_3O_4, Fe_2O_3 and $FeOOH/Fe(OH)_3$, and an inner layer, rich in Cr species containing Cr oxides and hydroxides.

3.2. Electrochemical measurements

3.2.1. Capacitance measurements (Mott-Schottky plots)

It is known that the oxides film formed on metal behaves as extrinsic semiconductor when exposed to an aqueous solution, owing to the presence of point defects in the crystals of film layer. The semiconductor behaviour and electronic properties of the surface film can be assessed by capacitance measurements. The relationship between the determined capacitance of the passivated electrode/electrolyte interface, C, and the applied potential, E, is described by the well known Mott-Schottky equation, neglecting the capacitance of the Helmholtz layer and surface states contribution for the total capacitance when the space charge region of a passive film semiconductor under depletion conditions [33]:

$$\frac{1}{C^2} = \frac{2}{\varepsilon\varepsilon_0 qN}\left(E - E_{FB} - \frac{kT}{q}\right) \quad (1)$$

where ε is the dielectric constant of the passive film (ε generally has values of 12.0 [34] and 15.6 [33,35] for the oxides films formed on carbon steels and alloy steels, respectively) and ε_0 the vacuum permittivity ($\varepsilon_0 = 8.85 \times 10^{-14}\,F\,cm^{-1}$), N is the carrier concentration (the donor density for n-type semiconductors or the acceptor density for p-type semiconductors), q is the elementary charge (+e for electrons and −e for holes, $e = 1.602 \times 10^{-19}\,C$), k is the Boltzmann constant ($k = 1.38 \times 10^{-23}\,J\,K^{-1}$) and T the absolute temperature (the KT/q term can be neglected because it is only approximately 25 mV at room temperature), E_{FB} is the flat band potential. According to Eq. (1), there is a linear relationship between C^{-2} and E, and for C^{-2} vs. E plots, a negative slope is for a p-type semiconductor response, inversely proportional to the acceptor concentration N_a, while a positive slope for n-type semiconductor, directly proportional to the concentration of donor N_d. And the E_{FB} can be calculated from the intercept of C^{-2} vs. E linear portion extrapolating with the potential axis.

Fig. 5 displays the Mott-Schottky plots for the films formed on CR and PC steel after 3 d immersion in solutions of different pH. It can be observed that in the Mott-Schottky plots for CR steel (Fig. 5a), two linear regions are presented, above and below the flat band potential that changes with pH, indicating the passive film formed on CR steel behaves as both n-type (positive slope) and p-type (negative slope) semiconductors, which is similar to passive films formed on stainless steels [35,36]. The duplex semiconductor character of the passive film on CR steel is related to its chemical composition. Its n-type semiconductor behaviour can be attributed to an outer region mainly composed of Fe oxides, and p-type semiconductor behaviour accounts for an inner region essentially formed of Cr species, according to previous investigations [35,36]. The passive film on PC steel does not present p-type semiconductivity since only one linear region with positive slope which suggests

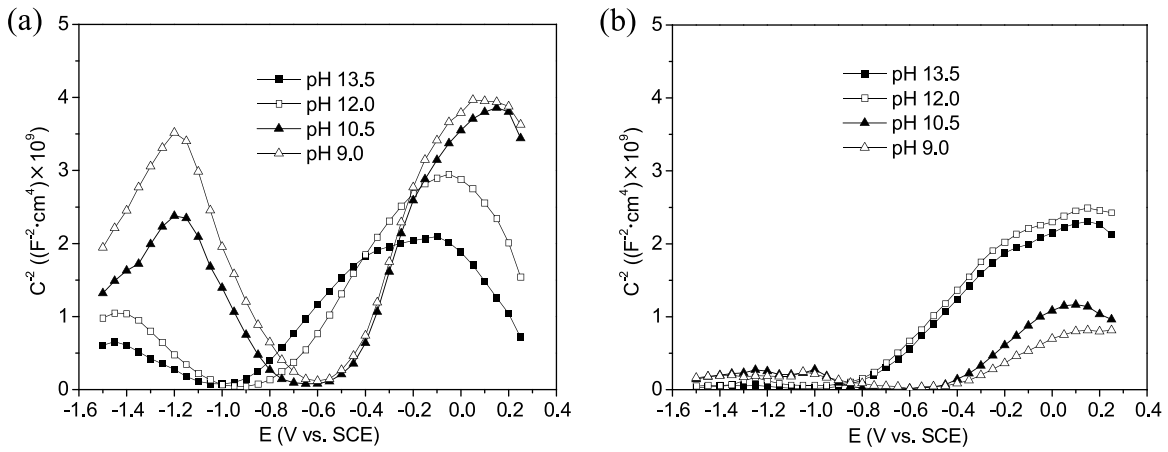

Fig. 5. Mott-Shottky plots for passive films formed on the steels in test solutions with different pH at immersion time of 3 d: (a) CR and (b) PC.

Table 3
Effect of pH values on semiconducting properties of passive films formed on the two steels in the solutions.

pH	CR			PC		
	N_d (10^{20} cm^{-3})	N_a (10^{20} cm^{-3})	E_{FB} (V vs. SCE)	N_d (10^{20} cm^{-3})	N_a (10^{20} cm^{-3})	E_{FB} (V vs. SCE)
13.5	25.11	58.04	−0.95	41.39	–	−0.94
12.0	19.03	34.84	−0.85	35.24	–	−0.85
10.5	11.75	16.39	−0.59	58.03	–	−0.57
9.0	10.09	11.47	−0.57	80.08	–	−0.55

an n-type semiconducting behaviour, can be observed in Fig. 5b. This consequence is of being expected, because the capacitance response is controlled only by the electronic structure of Fe species in the passive film.

The values of carrier concentrations (donor and acceptor species, i.e. N_d and N_a, respectively) and flat band potentials (E_{FB}) for semiconductive passive films formed on the two steels, are listed in Table 3. For the passive films on CR and PC steel in test solutions of different pH, the flat band potential which determines the position of energy bands with respect to the redox potentials of electroactive ions in the electrolyte [37], increases with pH decreasing, indicating the position of energy bands undergoes a positive shift gradually. This may be associated with the decreasing content of Fe^{2+} with pH dropping, which is assumed as the main doping species [38] in the films. N_d has the highest value for CR steel at pH 13.5 and for PC steel at pH 9.0, indicating a highly disordered nature of the passive films but separate mechanisms. For CR steel passive film formed at pH 13.5 has highest content of Fe^{2+}, resulting in higher doped density, while for PC steel passive film formed at pH 9.0 is highly defective and porous although with the Fe^{2+} content lowest. In the region of p-type semiconductivity for the passive film formed on CR steel, the slope sharpens appreciably as the pH decreases, and in accordance the N_a value shift substantially, meaning the film behaves as p-type semiconductor with poorer electrical conductivity. Such behaviour, which is the most remarkable at pH 9.0, is the characteristic of Cr oxides increasing enrichment in the film, and this results in higher resistance to the flow of electrons and holes [33].

3.2.2. Potentiodynamic polarization behaviour

Fig. 6 shows the d.c. anodic potentiodynamic polarization curves for CR and PC steel immersed for 3 d in solutions with pH varying from 13.5 to 9.0. In general, the polarization curves are quite similar, as a passive region where current density is almost constant could

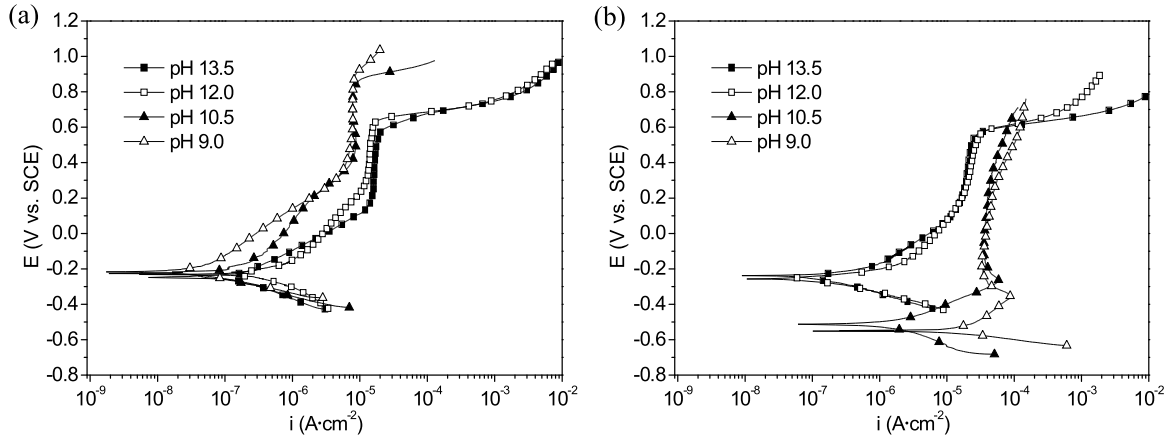

Fig. 6. Potentiodynamic polarization curves obtained in the anodic direction for the steels in test solutions with different pH after 3 d immersion: (a) CR and (b) PC.

Table 4
Electrochemical parameters derived from the polarization curves of the steels in test solutions with different pH after 3 d immersion.

	pH	E_{corr} (mV vs. SCE)	I_{corr} (A cm^{-2})	i_p (A cm^{-2})	E_{cp} (mV vs. SCE)	E_{tp} (mV vs. SCE)
CR	13.5	−247.8	1.34×10^{-7}	1.63×10^{-5}	150.8	576.1
	12.0	−231.2	1.08×10^{-7}	1.40×10^{-5}	269.7	633.9
	10.5	−227.6	5.31×10^{-8}	8.18×10^{-6}	388.1	862.0
	9.0	−218.1	2.53×10^{-8}	7.42×10^{-6}	398.5	878.6
PC	13.5	−240.6	1.51×10^{-7}	1.95×10^{-5}	146.7	563.7
	12.0	−258.4	1.67×10^{-7}	2.16×10^{-5}	188.6	568.2
	10.5	−512.3	1.24×10^{-6}	–	–	–
	9.0	−549.2	5.23×10^{-6}	–	–	–

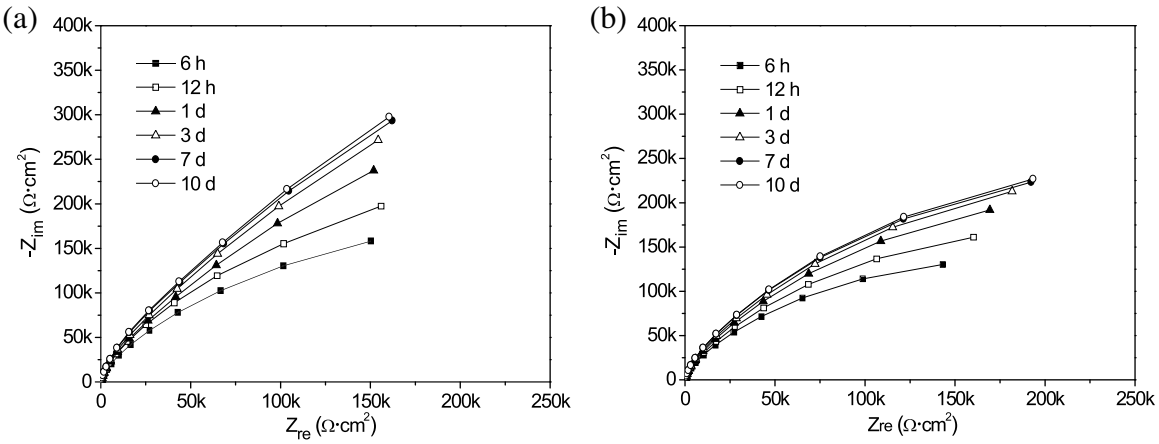

Fig. 7. EIS of the steels in test solution with pH 13.5 at different immersion time: (a) CR and (b) PC.

be observed and also a sharp increase in current density resulting from the onset of pitting corrosion presents in the curves, suggesting that the kinetics of the corrosion processes is basically identical. Of course, the cases for carbon steel at pH 10.5 and 9.0 are exception, which show a very different anodic behavior in the active dissolution region. Table 4 summarizes the corrosion potentials (E_{corr}), corrosion current densities (i_{corr}), critical passive potentials (E_{cp}), passive current densities (i_p) and breakdown potentials (E_{tp}) obtained from the polarization curves for CR and PC steel in solutions of different pH.

As shown in Fig. 6 and Table 4, in solutions with the same pH, compared to PC steel, CR steel has higher corrosion potentials, wider passive domain and lower corrosion and passive current densities, indicating better passive performances. Obviously, this is related to the differences between the constitutes and structures of the passive films on the two steels. A Cr-containing layer is formed in passive film of CR steel, improving the film corrosion resistance [39].

An important feature worthy of note is that the passivity evolution of the two steels with the pH varying is the opposite. For PC steel, the passivity is certainly declined by carbonation and almost vanishes at pH below 10.5. In fact, an increased pH favors the stability and lower dissolution rate of Fe oxides and hydroxides, leading to a thicker passive film on carbon steel [40]. However, for CR steel, the passivity is increasing, not weakening with the pH decreasing. The passive domain revealed by the polarization curves is wider, and E_{tp} and E_{corr} become more positive at the lower pH. The corrosion and passivation current densities both show a reduction of almost one order of magnitude from pH 13.5–9.0. All these evidence that for CR steel in alkaline solutions, less alkalinity offers better conditions for a higher protective passive film forming. This "abnormality" probably accounts for the increasing enrichment of more protective Cr species in the passive film on CR steel when the pH decreases, as shown by XPS.

Thus, it may be speculated that the alkalinity decreasing in media simulating concrete carbonation process, does not have negative effects on the corrosion resistance of Cr10Mo1 corrosion-resistant steel (if the environment is not contaminated by chlorides). This is a fine advantage compared to carbon steel, which maintains good passivity strongly depending on high pH and fails in passivation when pH goes down to 10.5. Freire et al. [41] observed the similar results for the effects of pH on passive behaviour of AISI 316 stainless steel in alkaline media, which confirms well the speculation above.

3.2.3. *Electrochemical impedance spectroscopy*

In this section the electrochemical behaviour of the surface films formed on CR and PC steel was assessed by electrochemical impedance spectroscopy (EIS). EIS data were recorded for all the electrodes after they were immersed in test solutions for 6 h, 12 h, 1 d, 3 d, 7 d, 10 d. Figs. 7 and 8 present the EIS response evolution of the films on the two steels in test solutions of different pH with immersion time. In general, the capacitance arc magnitudes of the two steels have an increasing over immersion time in solutions of pH 13.5 and 9.0. In fact, identical trend was reflected at all the pH values tested, implying the gradual growth of the surface film and an enhancement of its protection, as reported in other works [42]. However, the main changes of EIS spectra are observed during the first 3 days of immersion. After this period, and up to 10 days, the EIS spectra have very close profiles, indicating the passivation of the steels is completed and approaches to a basic steady-state after processing for 3 days in these conditions, which is compatible to the results reported in literatures [43,44].

Fig. 9 shows the EIS spectra (in Nyquist and Bode forms) obtained for CR and PC steel after 3 d immersion in solutions with pH from 13.5 to 9.0. It is evident that the changes of EIS spectra for the two steels with varying pH are materially different. For CR steel, the impedance response is increasing following the pH drop-

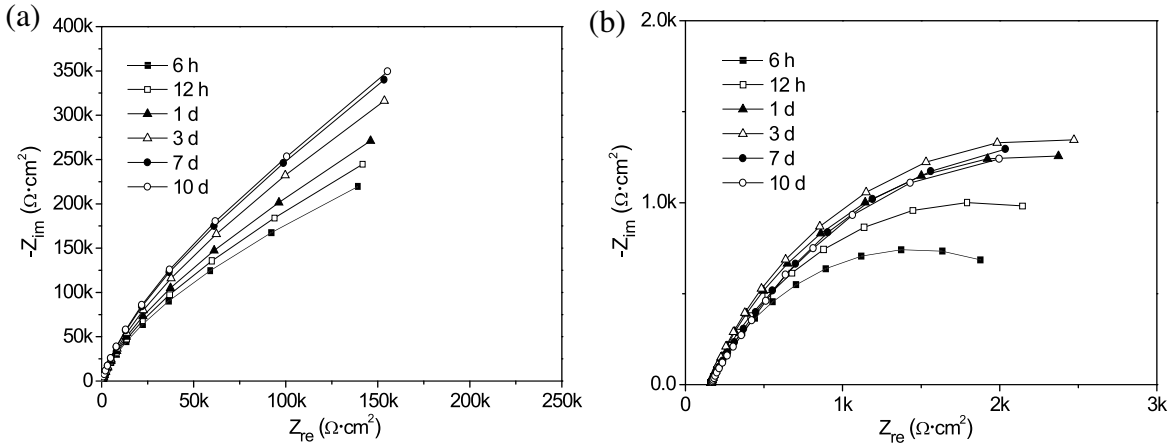

Fig. 8. EIS of the steels in test solution with pH 9.0 at different immersion time: (a) CR and (b) PC.

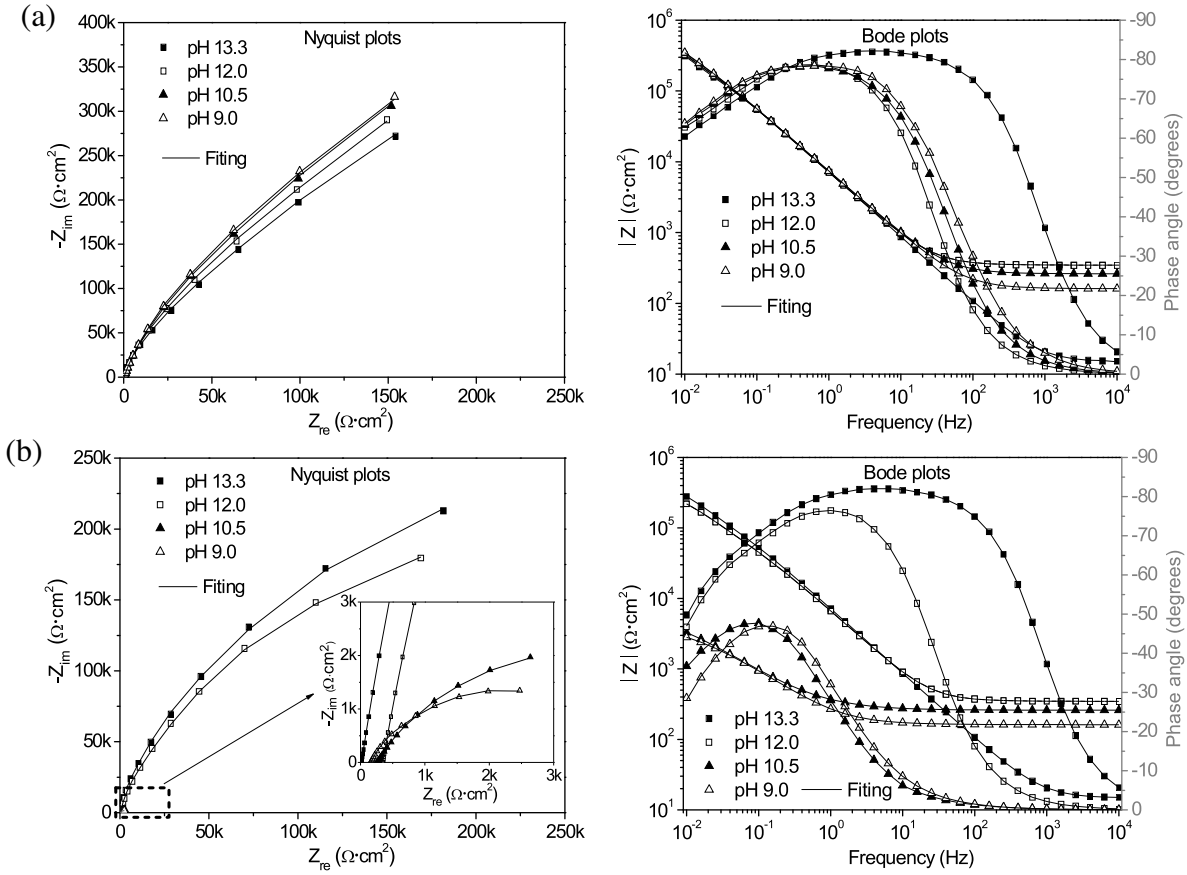

Fig. 9. EIS of the steels in test solutions of different pH after 3 d immersion: (a) CR and (b) PC.

ping, and the capacitance arc magnitude and overall impedance are even lager at pH 9.0, indicating the film formed at lower pH exhibits more protective behaviour. While for PC steel, the capacitance arc magnitude and overall impedance, as expected, markedly reduce under gradual carbonation, and could be almost negligible when the pH falls below 10.5, signifying that carbon steel hardly passivates in low pH media, which is also evidenced by the insignificant modulus of the phase angle maxima. The EIS results for CR and PC steel are basically accordant with the capacitance measurements and polarization curves.

For more detailed information on the electrochemical processes associated with the surface films with pH variation, the EIS results were fitted using equivalent circuits. Different models had been proposed for interpreting impedance data on passive behaviour of steels in alkaline media. Based on some trials and literatures support [20,21,41], the equivalent circuit depicted in Fig. 10a was adopted to fit the experimental data, which provided a right fitting as shown in Fig. 10b as an example with the small relevant errors (Fig. 10c).

Constant phase element (CPE) is used for the description of frequency dispersion behaviour corresponding to metal surface

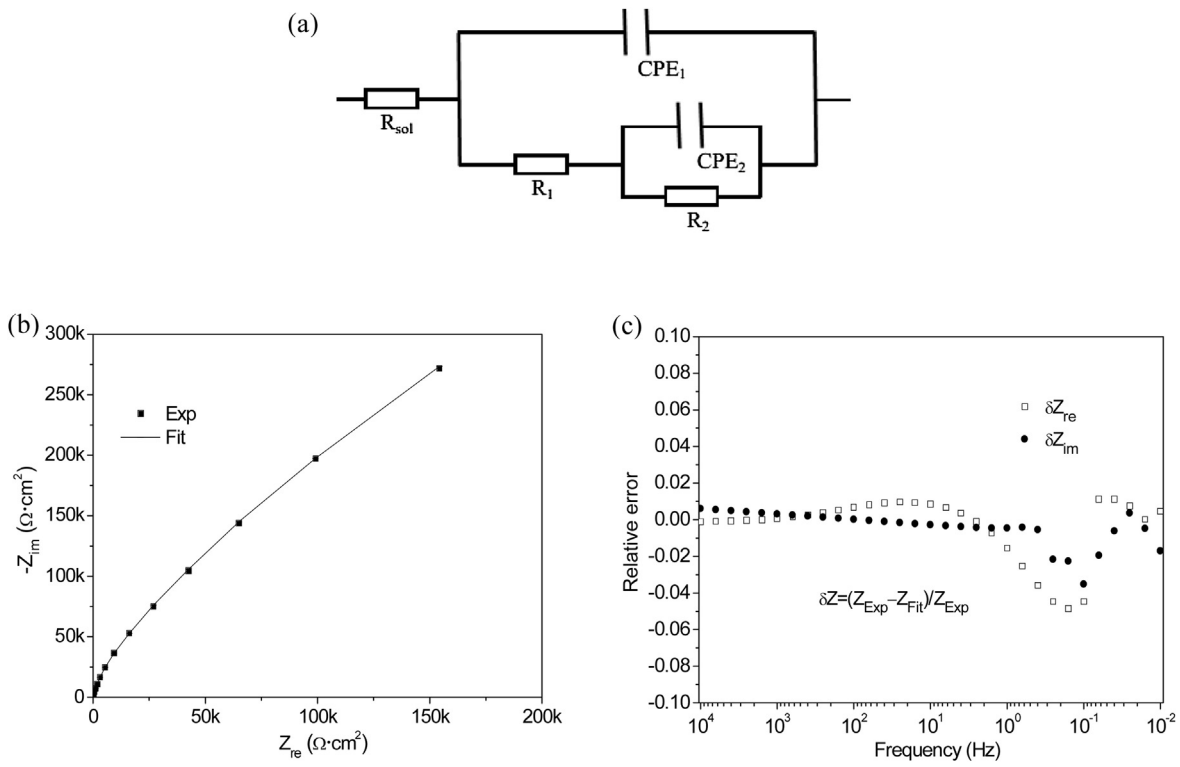

Fig. 10. The equivalent circuit used to model the experimental EIS data and fitting errors (taking CR steel in test solution of pH 13.5 at the immersion time of 3 d as an example): (a) equivalent circuits, (b) experimental data and fitting results comparison and (c) error plots.

Table 5
Best fitting parameters for the experimental EIS data obtained for the steels in solutions with different pH at immersion time of 3 d.

	pH	R_{sol} (Ω cm^2)	R_1 (Ω cm^2)	CPE_1		R_2 (Ω cm^2)	CPE_2	
				Y_0 (Ω^{-1} cm^{-2} s^n)	n		Y_0 (Ω^{-1} cm^{-2} s^n)	n
CR	13.5	15.1	2.91×10^5	2.34×10^{-5}	0.92	10.14×10^5	1.89×10^{-5}	0.83
	12.0	346.4	4.23×10^5	2.48×10^{-5}	0.91	13.47×10^5	1.78×10^{-5}	0.82
	10.5	261.7	6.52×10^5	2.58×10^{-5}	0.89	16.32×10^5	1.70×10^{-5}	0.80
	9.0	160.9	7.97×10^5	2.62×10^{-5}	0.89	18.76×10^5	1.67×10^{-5}	0.81
PC	13.5	14.9	1.97×10^5	2.56×10^{-5}	0.92	4.07×10^5	1.97×10^{-5}	0.82
	12.0	345.6	1.41×10^5	2.67×10^{-5}	0.91	3.16×10^5	2.16×10^{-5}	0.81
	10.5	260.4	2.02×10^3	1.26×10^{-3}	0.71	3.89×10^3	1.09×10^{-3}	0.62
	9.0	161.3	1.81×10^3	1.38×10^{-3}	0.72	2.52×10^3	1.02×10^{-3}	0.59

heterogeneity resulting from various physical phenomena [45]. The impedance of the CPE is defined by Eq. (2):

$$Z_{CPE} = \frac{1}{Y_0(jw)^n} \quad (2)$$

where Y_0 is the CPE electrical constant admittance, ω is the angular frequency (in rad/s), j is the imaginary number ($j^2 = -1$) and n is the CPE exponent, an adjustable parameter that always lies from 0 to 1. The interpretation of CPE parameter depends on n value. Intermediate n values are related to the non-homogeneities and roughness of the surfaces.

For the meaning of the circuit elements in this circuit model, the following physical interpretation is adopted [20,21,41]. The resistance connected in series with two time constants corresponds to the ohmic resistance of the solution (R_{sol}). The high frequency time constant (R_1, CPE_1) can be attributed to the charge transfer processes in the active surface areas (film defects/pores) and it is represented by the charge transfer resistance (R_1) coupled with the double layer capacitance (simulated by CPE_1). The low frequency time constant (R_2, CPE_2) is assigned to the redox processes taking place in the areas covered with the passive film (protective oxides) and it is composed of the passive layer resistance (R_2) and the passive film capacitance (CPE_2).

Table 5 presents the fitting parameters (based on the circuit model depicted in Fig. 10a) obtained from the experimental EIS spectra of the two steels in test solutions of different pH after 3 d immersion. It can be observed that for CR steel, as the pH drops, the R_1 value increases substantially, revealing that the charge transfer processes become more difficult. This probably is ascribed to the further growth and formation of more stable Cr oxides on the metal in less alkaline media, which could retard the Fe^{2+} in active areas to be released. The resistance R_2 also shows a similar evolution, with higher values at lower pH, evidencing the presence of a surface film that provides higher resistance to the flow of electrons in the redox processes. The CPE_2 evolution with pH reveals the surface film formed at lower pH performs heightened capacitive behaviour. The CPE_1 shows an upward tendency following the pH decreasing, meaning the more significant dispersion effect of the double layer capacitance. This may be related to the film surface roughing as more porous and loose FeOOH/$Fe(OH)_3$ forms in the layer under carbonation. Even so, the film formed on CR steel at lower pH has greater protection, for its higher polariza-

tion resistance R_p ($R_p = R_1 + R_2$), which has been widely used to account for the kinetics of electrochemical corrosion [46]. For PC steel, the R_1 and R_2 reduce about two orders of magnitude when the pH falls from 13.5 to 9.0, and the two time constants change dramatically. All these signify that the overall film become more and more defective because protective Fe oxides in the film layer decompose gradually with pH dropping, which results in cathode areas more approachable to accomplish depolarization and more active anode areas.

4. Conclusions

The electrochemical behaviour of passive films formed on alloy corrosion-resistant steel Cr10Mo1 in comparison with plain carbon steel in alkaline solutions of different pH (from 13.5 to 9.0) without chlorides contamination was evaluated by potentiodynamic polarization, electrochemical impedance spectroscopy and capacitance measurements, supplemented by the chemical composition analysis of the films using XPS and SIMS measurements. Analytical and electrochemical results evidenced that the composition and electrochemical response of the surface film formed changes notably as pH varying. The main conclusions obtained from this work are presented below:

The passive film formed on Cr10Mo1 steel consists of both Fe and Cr oxides/hydroxides, exhibiting a bilayer structure with an outer layer enriched in Fe oxides and hydroxides, and an inner layer mainly containing Cr species, while the film formed on carbon steel only includes Fe species with different oxidation states. As pH drops, for Cr10Mo1 steel and carbon steel the Fe^{2+}/Fe^{3+} ratio decreases continuously accompanied by the resolution of Fe oxides, while Cr species have a gradual enrichment in the film following the further growth and formation of more stable Cr oxides on the Cr10Mo1 metal. This results in great differences between the passive behaviour of the two steels in alkaline media of different pH.

The electrochemical measurements in a good agreement shows that, with pH decreasing, Cr10Mo1 steel bears enhanced passivity, signifying less alkalinity offers better conditions for a higher protective passive film forming, however, carbon steel has a significantly declined passivity and hardly passivates when pH below 10.5, as expected. For Cr10Mo1 steel, at high pH good passivity suggests the stability of the Fe species, and at lower pH increasing corrosion resistance reflects the formation of a surface film richer in Cr oxides. However, for carbon steel, lower the pH, lower the corrosion resistance of the surface film, due to the gradual destruction of protective Fe oxides under progressive carbonation.

Generally, the corrosion-resistant steel Cr10Mo1 has excellent passivity at all the pH values tested, for which, besides the Fe oxides, the Cr oxides in the film also play an important role and this is more significant in low pH environments. Compared to carbon steel, Cr10Mo1 steel shows a characteristic of self-reinforcing passivity against carbonation. The mechanism responsible for that is when pH drops, highly protective Cr oxides get increasingly enriched in the inner region of the film, providing the film higher corrosion resistance and less conductivity, although protective Fe oxides concentrated in the outer layer of the film decompose gradually.

Acknowledgments

The authors gratefully acknowledge the financial support from National Basic Research Program of China (No. 2015CB655100), National Natural Science Foundation of China (Nos. 51278098 and 51308111), Industry-University-Research Cooperative innovation fund of Jiangsu Province (No. BY2013091) and Transformation Projects of Major Scientific and Technological Achievements of Jiangsu Province (No. 85120000220).

References

[1] J.G. Cabrera, Deterioration of concrete due to reinforcement steel corrosion, Cem. Concr. Compos. 1 (1996) 47–59.
[2] J.L. Pandey, M.K. Banerjee, Concrete corrosion and reference practices—an overview, Anti Corros. Methods Mater. 45 (1998) 5–15.
[3] J.P. Broomfield, Steel Corrosion in Concrete—Understanding, Investigation and Repair, 2nd ed., Taylor & Francis, London, 2007.
[4] B. Benmokrane, O. Chaallal, R. Masmoudi, Glass fiber reinforced plastic (GFRP) rebars for concrete structures, Constr. Build. Mater. 6 (1995) 353–364.
[5] S. Sawada, C.L. Page, M.M. Page, Electrochemical injection of organic corrosion inhibitors into concrete, Corros. Sci. 47 (2005) 2063–2078.
[6] D.W. Pfeifer, High performance concrete and reinforcing steel with a 100-year service life, PCI J. 45 (2000) 46–54.
[7] F.N. Smith, M. Tulimin, Using stainless steel as long-lasting rebar material, Mater. Perform. 38 (1999) 72–76.
[8] F. Presuel-Moreno, J.R. Scully, S.R. Sharp, Literature review of commercially available alloys that have potential as low-cost, corrosion-resistant concrete reinforcement, Corrosion 66 (2010) 1–13.
[9] N.R. Baddoo, Stainless steel in construction: a review of research, applications, challenges and opportunities, J. Constr. Steel Res. 64 (2008) 1199–1206.
[10] G.G. Clemena, Y.P. Virmani, Comparing the chloride resistances of reinforcing bars: evaluating new, economical metallic reinforcement for its ability to withstand high salt concentrations, Concr. Int. 26 (2004) 39–49.
[11] Y. Chen, Z.M. Yang, H.M. Wang, Comprehensive properties of 400 MPa grade corrosion-resistant rebar, J. Iron Steel Res. Int. 19 (2012) 48–52.
[12] MMFX Steel Corporation of America. MMFX steel 2002, product bulletin, http://www.mmfxsteel.com (2002).
[13] M.F. Hurley, Corrosion Initiation and Propagation Behavior of Corrosion-resistant Concrete Reinforcing Materials ,Ph.D. Thesis, University of Virginia, Charlottesville, 2007.
[14] M.F. Hurley, J.R. Scully, Threshold chloride concentrations of selected corrosion-resistant rebar materials compared to carbon steel, Corrosion 62 (2006) 892–904.
[15] Elstner Associates Incorporation, Comparative corrosion testing and analysis of MMFX 2 rebars for reinforced concrete applications, Final Report WJE No. 2003.0707.0, Illinois (2008).
[16] A.A. Sagüés, Modeling the effects of corrosion on the lifetime of extended reinforced concrete structures, Corrosion 59 (2003) 854–866.
[17] N. Mohamed, M. Boulfiza, R. Evitts, Corrosion of carbon steel and corrosion-resistant rebars in concrete structures under chloride ion attack, J. Mater. Eng. Perform. 22 (2013) 787–795.
[18] J.C. Zhang, W.K. Huang, Y. Li, H. Ma, A highly corrosion-resistant reinforcing steel with high strength and its preparation technologies (in Chinese), Chinese Patent, CN103789677A (2014).
[19] M. Kouřil, P. Novák, M. Bojko, Threshold chloride concentration for stainless steels activation in concrete pore solutions, Cem. Concr. Res. 40 (2010) 431–436.
[20] F.L. Fei, J. Hu, J.X. Wei, Q.J. Yu, Z.S. Chen, Corrosion performance of steel reinforcement in simulated concrete pore solutions in the presence of imidazoline quaternary ammonium salt corrosion inhibitor, Constr. Build. Mater. 70 (2014) 43–53.
[21] R. Liu, L.H. Jiang, J.X. Xu, C.S. Xiong, Z.J. Song, Influence of carbonation on chloride-induced reinforcement corrosion in simulated concrete pore solutions, Constr. Build. Mater. 56 (2014) 16–20.
[22] X.G. Feng, Y.M. Tang, Y. Zuo, Influence of stress on passive behaviour of steel bars in concrete pore solution, Corros. Sci. 53 (2011) 1304–1311.
[23] H. Luo, C.F. Dong, K. Xiao, X.G. Li, Characterization of passive film on 2205 duplex stainless steel in sodium thiosulphate solution, Appl. Surf. Sci. 258 (2011) 631–639.
[24] C.T. Liu, J.K. Wu, Influence of pH on the passivation behavior of 254SMO stainless steel in 3.5% NaCl solution, Corros. Sci. 49 (2007) 2198–2209.
[25] C. Donik, A. Kocijan, J.T. Grant, M. Jenko, A. Drenik, B. Pihlar, XPS study of duplex stainless steel oxidized by oxygen atoms, Corros. Sci. 51 (2009) 827–832.
[26] M.F. Montemor, A.M.P. Simões, M.G.S. Ferreira, M. Da Cunha Belo, The role of Mo in the chemical composition and semiconductive behaviour of oxide films formed on stainless steels, Corros. Sci. 41 (1999) 17–34.
[27] H. Antony, L. Legrand, L. Maechal, S. Perrin, P. Dillmann, A. Chaussé, Study of lepidocrocite γ-FeOOH electrochemical reduction in neutral and slightly alkaline solutions at 25 °C, Electrochim. Acta 51 (2005) 745–753.
[28] M. Pourbaix, Atlas d'equilibres Electrochimiques, Gauthier-villars et Cie, Paris, 1963.
[29] S. Lozano-Perez, T. Yamada, T. Terachi, M. Schroder, C.A. English, G.D.W. Smith, C.R.M. Grovenor, B.L. Eyre, Multi-scale characterization of stress corrosion cracking of cold-worked stainless steels and the influence of Cr content, Acta Mater. 57 (2009) 5361–5381.
[30] M. Salasia, G.B. Stachowiak, G.W. Stachowiak, M.R. Kilburn, NanoSIMS investigation of passive oxide films on high-Cr cast iron, Corros. Sci. 67 (2013) 298–303.
[31] M. Mancio, G. Kusinski, P.J.M. Monteiro, T.M. Devine, Electrochemical and in-situ SERS study of passive film characteristics and corrosion performance

of 9%Cr micro-composite steel in highly alkaline environments, J. ASTM Int. 6 (2009) 1–10.
[32] N.E. Hakiki, Comparative study of structural and semiconducting properties of passive films and thermally grown oxides on AISI 304 stainless steel, Corros. Sci. 53 (2011) 2688–2699.
[33] N.E. Hakiki, S. Boudin, B. Rondot, M. Da Cunha Belo, The electronic structure of passive films formed on stainless steels, Corros. Sci. 37 (1995) 1809–1822.
[34] L. Hamadou, A. Kadri, N. Benbrahim, Characterisation of passive films formed on low carbon steel in borate buffer solution (pH 9.2) by electrochemical impedance spectroscopy, Appl. Surf. Sci. 252 (2005) 1510–1519.
[35] A. Di Paola, Semiconducting properties of passive films on stainless steels, Electrochim. Acta 34 (1989) 203–210.
[36] S. Ningshen, U.K. Mudali, V.K. Mittal, H.S. Khatak, Semiconducting and passive film properties of nitrogen-containing type 316LN stainless steels, Corros. Sci. 49 (2007) 481–496.
[37] S.R. Morrison, Electrochemistry at Semiconductor and Oxidized Metal Electrodes, Plenum Press, New York, 1980.
[38] M.J. Carmezim, A.M. Simões, M.F. Montemor, M. Da Cunha Belo, Capacitance behaviour of passive films on ferritic and austenitic stainless steel, Corros. Sci. 47 (2005) 581–591.
[39] C.O.A. Olsson, D. Landolt, Passive films on stainless steels-chemistry, structure and growth, Electrochim. Acta 48 (2003) 1093–1104.
[40] P. Ghods, Multi-scale Investigation of the Formation and Breakdown of Passive Films on Carbon Steel Rebar in Concrete, Ph.D. Thesis, Carleton University, Ottawa, 2010.
[41] L. Freire, M.J. Carmezim, M.G.S. Ferreira, M.F. Montemor, The passive behaviour of AISI 316 in alkaline media and the effect of pH: a combined electrochemical and analytical study, Electrochim. Acta 55 (2010) 6174–6181.
[42] S.M.A. Haleem, E.E. Abd El Aal, S. Abd El Wanees, A. Diab, Environmental factors affecting the corrosion behavior of reinforcing steel: I. The early stage of passive film formation in $Ca(OH)_2$ solutions, Corros. Sci. 52 (2010) 3875–3882.
[43] A. Poursaee, C.M. Hansson, Reinforcing steel passivation in mortar and pore solution, Cem. Concr. Res. 37 (2007) 1127–1133.
[44] M. Sánchez, J. Gregori, C. Alonso, J.J. García-Jareño, H. Takenouti, F. Vicente, Electrochemical impedance spectroscopy for studying passive layers on steel rebars immersed in alkaline solutions simulating concrete pores, Electrochim. Acta 52 (2007) 7634–7641.
[45] U. Rammelt, G. Reinhard, The influence of surface roughness on the impedance data for iron electrodes in acid solutions, Corros. Sci. 27 (1987) 373–382.
[46] H. Yu, H.X. Li, T. Zhou, B.L. Yin, S.J. Yin, Y.L. Zhang, Effect of tin on the corrosion behavior of sea-water corrosion-resisting steel, Mater. Des. 84 (2015) 1–9.